Journal of Catalysis 273 (2010) 18–28

Contents lists available at ScienceDirect

Journal of Catalysis

journal homepage: www.elsevier.com/locate/jcat

Effect of active sites for a water–gas shift reaction on Cu nanoparticles

Ching-Shiun Chen *, Tzu-Wen Lai, Chen-Chih Chen

Center for General Education, Chang Gung University, 259 Wen-Hwa 1st Road, Kwei-Shan Tao-Yuan 333, Taiwan, ROC

ARTICLE INFO

Article history:
Received 5 January 2010
Revised 21 April 2010
Accepted 22 April 2010
Available online 26 May 2010

Keywords:
Water–gas shift reaction
Copper nanoparticles
Atomic layer epitaxy
CO adsorption
Infrared spectroscopy

ABSTRACT

The effect on the water–gas shift reaction of active sites on Cu nanoparticles on silica prepared by atomic layer epitaxy was investigated. The Cu nanoparticles are proposed to contain two major active sites on the surface, defect sites on Cu particles (L_1 sites) and sites having strong interactions with oxide support on highly dispersed and/or isolated Cu particles (L_2 sites). The defect sites on the Cu nanoparticles induce intense dissociation of H_2O to form atomic oxygen, leading to the redox mechanism that occurred in the reaction. The atomic oxygen generated from H_2O on the defect sites has a high reactivity toward CO adsorbed onto L_1 and L_2 sites to form CO_2. The adsorption heats of CO adsorbed onto the L_1 and L_2 sites varying with coverage are obtained for coverage 0 and 1 with $E_0 = 51$ and $E_1 = 39$ kJ/mol for L_1-CO and $E_0 = 70$ and $E_1 = 46$ kJ/mol for L_2-CO.

1. Introduction

Copper catalysts, because of their proven activity for water–gas shift (WGS) and reverse water–gas shift (RWGS) reactions, which are relevant to several industrial processes [1–13], are usually preferred as the active component for such processes. The WGS reaction ($CO + H_2O \rightarrow H_2 + CO_2$) is used extensively in the conversion of fossil fuels to hydrogen [1–7]. In particular, the WGS reaction achieves the conversion of CO to CO_2, which is important when hydrogen is used as a clean fuel for proton-exchange membrane fuel cells, in view of the strong poisoning effect of CO on Pt-based anodes

The WGS reaction using Cu-based catalysts has been widely investigated with respect to factors such as the nature of supports [14–19], the effect of alloy formation [20], and the role of oxygen vacancies [4,21], but the effect of nanoparticles containing considerable numbers of defect sites, such as step and edge sites, still remains unclear. To date, preparations of small metallic particles have been extensively investigated in catalytic studies and are viewed as a very active area of research in solid-state physics and chemistry. Conventional supported catalysts are prepared by wet chemistry methods, which generate small and dispersed active catalytic sites but may suffer from uncontrollable size distribution. It has been noted that nanoparticles usually offer a higher surface-to-volume ratio and a higher concentration of partially coordinated surface sites compared to bulk materials and, consequently, appear to possess different physical and chemical properties [22,23]. Several studies mention that size reductions of metals can cause some changes in the electronic structure and the distribution of surface sites, leading to enhanced catalytic activity [24–26].

In our previous investigations, an alternative route for preparing uniform Cu nanoparticles on SiO_2, atomic layer epitaxy (ALE), was used; nanoparticles with an average diameter of 2.4–3.4 nm and a narrow size distribution (<10% root mean square diameter) were obtained [27,28]. The Cu nanoparticles prepared using the ALE method can have properties very different from those of typical Cu-based catalysts [8]. In general, Cu-based catalysts undergo deactivation at temperatures higher than 573 K, but the ALE-Cu/SiO_2 catalyst has sufficient thermal stability to prevent sintering at 773 K [8]. The ALE technique is a surface-controlled, layer-by-layer process that deposits thin films at an atomic scale through self-limiting surface reactions [29]. This technique for catalyst preparation is very different from the traditional impregnation method, in which the gaseous copper precursor ($Cu(thd)_2$) must be deposited on SiO_2 support at 433–463 K. In other words, a strong interaction between $Cu(thd)_2$ and SiO_2 may occur, evidenced by the high-temperature peak in TPR profiles [27]. The reason for the highly thermal stability of ALE-Cu/SiO_2 is not fully understood, but we assume that it may depend on the strong interaction between $Cu(thd)_2$ and SiO_2.

On the other hand, the Cu nanoparticles of the ALE-Cu/SiO_2 catalyst can strongly bind CO and have surprisingly better performance in WGS and RWGS reactions than Pt and Pd catalysts [8,27,28]. ALE-Cu/SiO_2 containing a low copper concentration revealed the effect of the Cu nanoparticles, showing dramatically high activity for the WGS reaction in comparison with a 10.3% IM-Cu/SiO_2 catalyst prepared by an impregnation method and a commercial 20% Cu/ZnO/Al_2O_3 catalyst, even at room temperature

* Corresponding author. Fax: +886 32118700.
E-mail address: cschen@mail.cgu.edu.tw (C.-S. Chen).

0021-9517/$ - see front matter © 2010 Elsevier Inc. All rights reserved.
doi:10.1016/j.jcat.2010.04.019

[27]. The 10.3% IM-Cu/SiO_2 gave a copper surface area similar to that of 2.5% ALE-Cu/SiO_2 but exhibited very weak catalytic activity. The 10.3% IM-Cu/SiO_2 catalysts revealed no detectable activity below 423 K.

The active sites on the ALE-Cu/SiO_2 surface are discriminated by CO infrared adsorption spectra, suggesting two possible major active sites on the copper surface, defect sites and sites with highly dispersed Cu particles and/or isolated Cu atoms [27]. Our previous study determined that the defect sites on the ALE-Cu/SiO_2 catalyst are of fundamental importance in the catalytic activity of the WGS reaction. However, determination of the role of the active sites in the WGS reaction and fundamental characterization of sites on the Cu nanoparticles has not been performed. In this paper, we further discuss the intrinsic activity of active sites on Cu nanoparticles for the WGS reaction. The silica support is used to disperse the Cu particles, because the material cannot participate in the WGS reaction.

In situ FT-IR spectroscopy under dynamic conditions can create a controlled gas–solid surface state for catalytic reactions. It can provide a powerful technique for investigation of the surface state of the catalyst and for characterization of the adsorbed species formed by the WGS reaction. CO chemisorption on the metal particles is the first surface elementary step for the WGS reaction involving CO. The adsorption heat of CO chemisorption may be a key parameter for realizing the fundamental properties of active sites and the contribution of CO adsorbed onto different sites during the reaction. Recently, the analytic procedure of adsorption equilibrium infrared spectroscopy (AEIR), derived from FT-IR spectroscopy, was successfully developed by Bianchi and coworkers [30–40], providing a meaningful technique to determine the adsorption heat of CO on metal surfaces with varying coverage, based on the dependence between CO coverage and adsorption temperature. In this study, *in situ* FT-IR spectroscopy, temperature-programmed reduction (TPR), and activity tests of the WGS reaction are used to demonstrate the roles of active sites in the WGS reaction and a redox mechanism for the reaction pathway of the ALE-Cu/SiO_2 catalyst; the heat of CO adsorption on different sites is also determined using the AEIR method to characterize the major active sites.

2. Experimental

2.1. Catalyst preparation

The ALE-Cu/SiO_2 catalysts were prepared using F-120C ALE equipment (Microchemistry Ltd.). Growth experiments were performed in a flow-type reactor at low pressure, with nitrogen as the carrier gas. In each run, 2–3 g of SiO_2 support was used. A SiO_2 support with a surface area of 300 m^2/g was used for the ALE samples and purchased from Aldrich. The SiO_2 support was preheated at 673 K for 16 h to stabilize the number of bonding sites and to remove physisorbed water. $Cu(thd)_2$ (thd = 2,2,6,6-tetramethyl-3,5-heptanedionate) was introduced at 413 K. The $Cu(thd)_2$ was then deposited on the SiO_2 support at 463 K over a reaction time of 8 h.

Two kinds of reduction pretreatments for ALE-Cu/SiO_2 catalysts were used in this study. Low-temperature reduction was performed by calcination in air and by reduction in H_2 gas at 573 K for 5 h. The high-temperature reduction was carried out according to the following sequence of steps: (1) calcination at 573 K in air for 5 h; (2) reduction by temperature-programmed reduction in 10% H_2/N_2 gas from 298 to 973 K; and (3) reduction at 773 K in H_2 gas for 5 h.

2.2. Catalytic activity measurements

All WGS reactions were carried out in a fixed-bed reactor (0.95-cm outer diameter) at atmospheric pressure. A thermocouple connected to a PID temperature controller was placed on top of the catalyst bed. Samples (50 mg) of catalyst were used for all WGS reactions, which were conducted at ambient pressure and temperature (373–473 K). A syringe pump was used to control the feeding rate of water at 1–3 ml/h. The liquid water in the flowing system with heating belts was vaporized to gas before entering the reactor. The reactions were performed by mixing a 5% CO/He stream (50 ml/min) with gaseous H_2O over 50 mg of catalyst. All products were analyzed by gas chromatography (GC) on a 12-ft Porapak-Q column using a thermal conductivity detector (TCD). The turnover frequency (TOF) was calculated by the formula [41] TOF = [conversion $\times$ 0.25 (ml/s for CO) $\times$ 6.02 $\times$ 10^{23} (molecules/mol)]/[24,400 (ml/mol) $\times$ 1.46 $\times$ 1019 (Cusites/m^2)].

2.3. H_2 temperature-programmed reduction (H_2-TPR)

H_2-TPR of catalysts was performed at atmospheric pressure in a conventional flow system. The ALE-Cu/SiO_2 catalyst was placed in a tube reactor and heated in a 10% H_2/N_2 mixed gas stream flowing at 30 ml/min at a heating rate of 10 K/min. The TCD current was 80 mA, and the detector temperature was 373 K. A cold trap containing a gel formed by adding liquid nitrogen to isopropanol in a Thermos flask was used to prevent water from entering the TCD.

2.4. Measurements of FT-IR spectra

In situ DRIFT analysis of CO adsorption and CO/H_2O coadsorption on ALE-Cu/SiO_2 was performed with a Nicolet 5700 FT-IR spectrometer fitted with a mercury cadmium telluride detector operating at resolution 1 cm^{-1} and 256 scans. The DRIFT cell (Harrick Co.) was equipped with ZnSe windows and a heating cartridge that allowed samples to be heated to 773 K.

2.5. Measurement of the copper surface area

The specific Cu^0 surface area and dispersion of Cu catalysts were determined by N_2O chemisorption and TPR. The Cu catalyst was reduced at 773 K in H_2 gas for 5 h, and then all Cu^0 on the catalysts was carefully oxidized in a 10% N_2O/N_2 stream according to the reaction $2Cu_{(s)} + N_2O \rightarrow Cu_2O_{(s)} + N_2$. The monolayer of Cu_2O on the catalyst surface after N_2O chemisorption was reduced using a TPR process. N_2O chemisorption was performed with a 10% N_2O/N_2 mixture flowing at 30 ml/min at 353 K. The TPR area of Cu_2O was quantified by sampling 1 ml of 10% H_2/N_2 to calculate the amount of N_2O consumed. The Cu^0 surface area could thus be calculated, assuming a N_2O/Cu molar stoichiometry of 0.5. The average surface density for Cu metal is 1.46 $\times$ 10^{19} copper atoms/m^2. The copper content of all catalysts was measured by inductively coupled plasma mass spectrometry. As the number of Cu atoms on the surface and the total Cu content of the catalyst were known, the copper dispersion could thus be calculated. The average particle size of Cu was calculated from the Cu surface area by the formula $d = 6\ V/A$. A 40% dispersion, 6.5 m^2/g Cu surface area, and 2.9 ± 0.29-nm Cu particle size were obtained for the 2.5% ALE-Cu/SiO_2 catalyst [28].

3. Results

3.1. FT-IR of CO and H_2O coadsorbed onto ALE-Cu/SiO_2

In situ FT-IR spectroscopy was used to investigate the CO and H_2O coadsorbed onto Cu nanoparticles at 298 K in order to observe the important intermediate occurred in the transient reaction. Fig. 1 displays the spectra obtained in time-dependence studies of the reaction of adsorbed H_2O on ALE-Cu/SiO_2 with CO gas at

298 K. Fig. 1 reveals the results obtained when a 5% CO/He stream was passed through an H_2O precovered ALE-Cu/SiO_2 surface. These findings show that the preadsorbed H_2O could react with CO, resulting in a new species on the surface with a peak at 1950 cm^{-1}. The preadsorption of H_2O was performed by injecting 5 μl of H_2O onto the clean ALE-Cu/SiO_2 surface after reduction pretreatment. In previous studies, it was speculated that the WGS reactions on the Cu surface might involve the formation of some intermediate such as formate, carbonate, or carboxyl species [6,42,43]. However, our study did not reveal similar phenomena for ALE-Cu/SiO_2 because no complicated IR spectra from a reaction intermediate could be found in the region of 1300–1800 cm^{-1} of Fig. 1 as H_2O vanished. A new peak at 1950 cm^{-1} could be formed in the course of the reaction but disappeared when a He stream passed through the reactor, as shown in spectrum (g).

Fig. 2 shows the IR spectra of CO adsorbed onto ALE-Cu/SiO_2 pretreated with H_2O. First, 5 μl of H_2O was dosed onto the Cu surface under a helium stream for 10 min as shown in spectrum (a), and then the catalyst was heated to 573 K to eliminate H_2O molecules from the Cu surface. Spectrum (b) shows that CO was adsorbed at 298 K onto the ALE-Cu/SiO_2 through H_2O adsorption and desorption processes. The characteristic IR peaks of CO_2 could be rapidly observed on the catalyst and were enhanced with increasing temperature.

3.2. FT-IR study of the WGS rate on ALE-Cu/SiO_2

The effect of the reduction temperature on the consumption of preadsorbed CO on ALE-Cu/SiO_2 after injection of 5 μl of H_2O to the reaction mixture is displayed in Fig. 3. Spectra (a) and (b) in Fig. 3A are the IR spectra of CO adsorbed onto the ALE-Cu/SiO_2 surface with reduction at 573 and 773 K. The IR band belonging to linear CO adsorption on the Cu surface could be fitted by two principal peaks, which revealed two major active sites on the copper surface: sites for L_1-CO with an IR spectrum at 2119 cm^{-1} and sites for L_2-CO with an IR spectrum at 2134 cm^{-1}. The L_1 and L_2 sites can be proposed to depend on the defect sites and on the highly dispersed supported copper particles, respectively, based on assignments of IR spectra in the literature [27].

The coverage of L_1- and L_2-CO declined with H_2O adsorption, as compared in Fig. 3B and C, showing that high-temperature reduction of the copper surface could provide a higher consumption rate for the L_1- and L_2-CO species than the low-temperature reduction of the copper surface. Additionally, the initial rate of the WGS reaction was further investigated at higher CO coverage. Spectrum (c) in Fig. 3A reveals that the adsorption of CO was obtained using the following steps: pure CO at 298 K for 30 min → pure CO at 673 K for 30 min → pure CO at 298 K for 30 min → He at 298 K for 30 min. The CO adsorption in spectrum (c) was enhanced by the aforementioned treatment. The differences in the IR spectrum between (c) and (b) are shown in spectrum (d), revealing that the CO-treatment process could promote CO adsorption on ALE-Cu/SiO_2 and could cause IR intensity to increase by 30%. It is noteworthy that CO-treatment could lead to a significant decrease of the rate of L_1-CO consumption (Fig. 3B), but the WGS rate of L_2-CO is similar to that of L_2-CO for surface reduction at 773 K (Fig. 3C). The measurement of Cu sites used in this study has been performed in our previous paper to have 9.5×10^{19} g^{-1} [8]. The ratio of relative intensity for L_1-CO/L_2-CO from the spectrum (c) in Fig. 3A can be obtained with 0.65/0.35, assuming that the CO-treatment leads to a saturated amount of CO adsorption. Therefore, the number of sites might be determined to 6.2×10^{19} g^{-1} for L_1 sites and 3.3×10^{19} g^{-1} for L_2 sites, respectively.

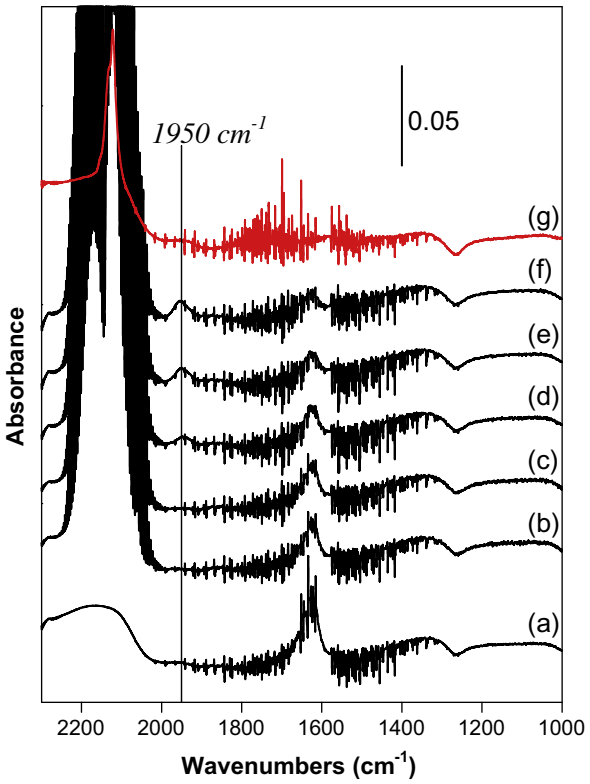

Fig. 1. Time-dependent IR spectra of the 5% CO/He stream passed through the ALE-Cu/SiO_2 catalyst with H_2O precovered by a 5-μl H_2O dosage at 298 K for (a) 0 min; (b) 5 min; (c) 10 min; (d) 30 min; (e) 60 min; (f) 75 min; (g) a pure He (20 ml/min) stream passed for 10 min after (f).

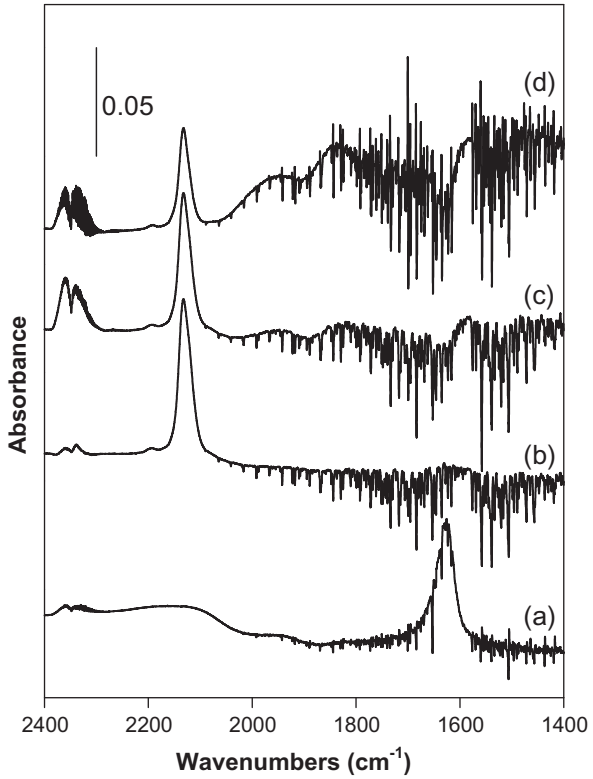

Fig. 2. IR spectra of CO adsorbed onto the ALE-Cu/SiO_2 catalyst containing H_2O covered at 298 K: (a) injection of 5 μl of H_2O onto the catalyst; after (a), the catalyst was heated to 573 K to remove all adsorbed H_2O from the Cu surface for CO adsorption at (b) 298 K; (c) heated to 323 K after (b); (d) heated to 348 K after (c). Adsorption of CO was performed by exposure to a 20 ml/min pure CO stream at atmospheric pressure for 30 min, followed by a 20 ml/min helium stream to purge the CO gas for 30 min at 298 K.

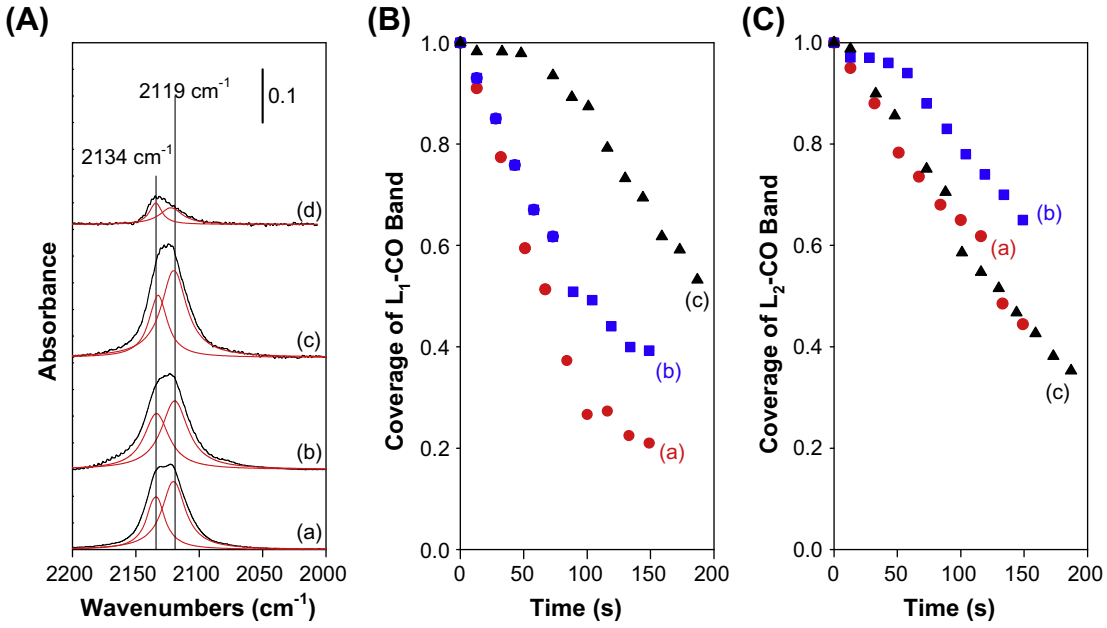

Fig. 3. (A) IR spectra of CO adsorbed onto differently pretreated ALE-Cu/SiO_2 catalysts: (a) catalyst reduction at 573 K; (b) catalyst reduction at 773 K; (c) adsorption of CO onto the ALE-Cu/SiO_2 catalyst obtained in the following procedure: pure CO at 298 K for 30 min → pure CO at 673 K for 30 min → pure CO at 298 K for 30 min → He at 298 K for 30 min; (d) difference of IR spectrum between curves (c) and (b). Time dependence of CO coverage for coadsorption of CO and H_2O in part (A) for (B) L_1-CO and (C) L_2-CO. The dosage of H_2O was 5 μl.

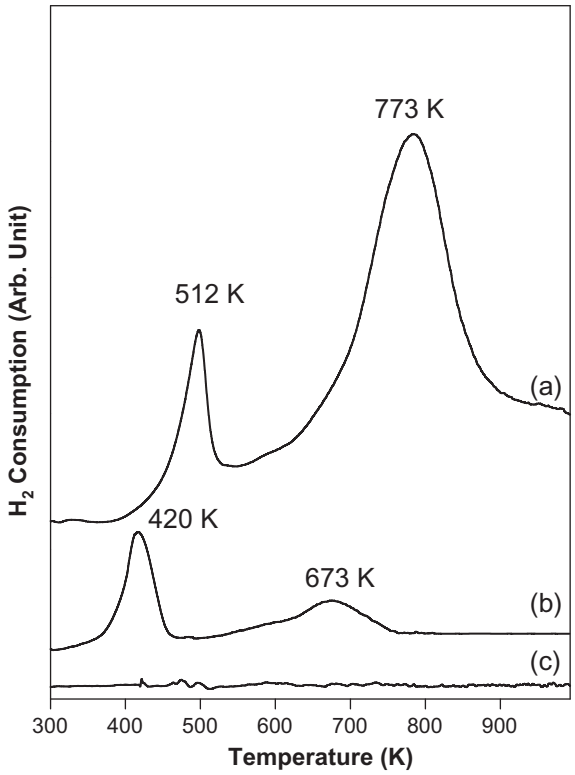

Fig. 4. TPR profiles of (a) the ALE-Cu/SiO_2 catalyst after calcination in air at 573 K for 5 h; (b) the reduced ALE-Cu/SiO_2 catalyst oxidized by a N_2O stream with 30 mL/min at 353 K for 180 s; (c) pure SiO_2 support.

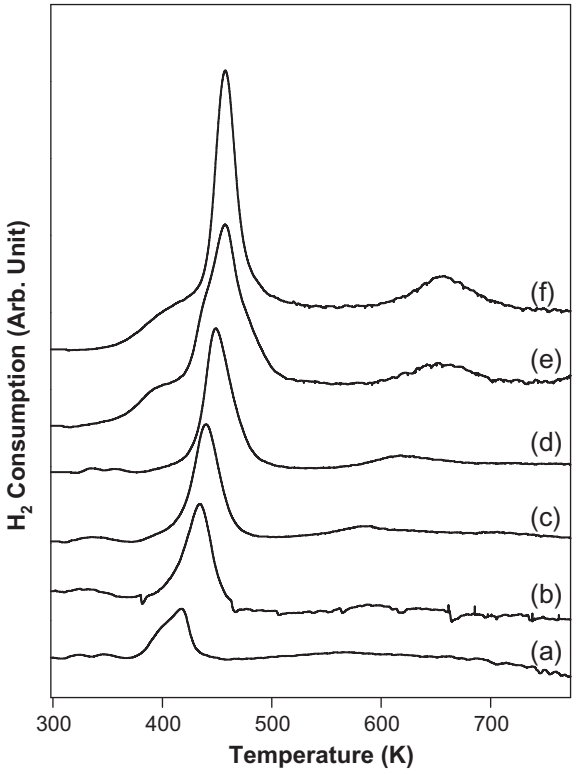

Fig. 5. TPR profiles of reduced ALE-Cu/SiO_2 treated by H_2O adsorption at (a) 298 K; (b) 323 K; (c) 348 K; (d) 373 K; (e) 423 K; (f) 473 K. The H_2O adsorptions at different temperatures were generated by a helium stream with a total flow rate of 30 ml/min passing through liquid water at room temperature and then passing the H_2O over 50 mg of catalyst for 1 h.

3.3. H_2-TPR of the ALE-Cu/SiO_2 catalyst

Fig. 4 compares the H_2-TPR profiles of the ALE-Cu/SiO_2 catalyst in calcination and N_2O oxidation treatment. According to our previous study, the H_2-TPR of the sample after calcination in air at 573 K for 5 h shows two major reduction peaks with maxima around 512 and 773 K in curve (a); these are attributed to the

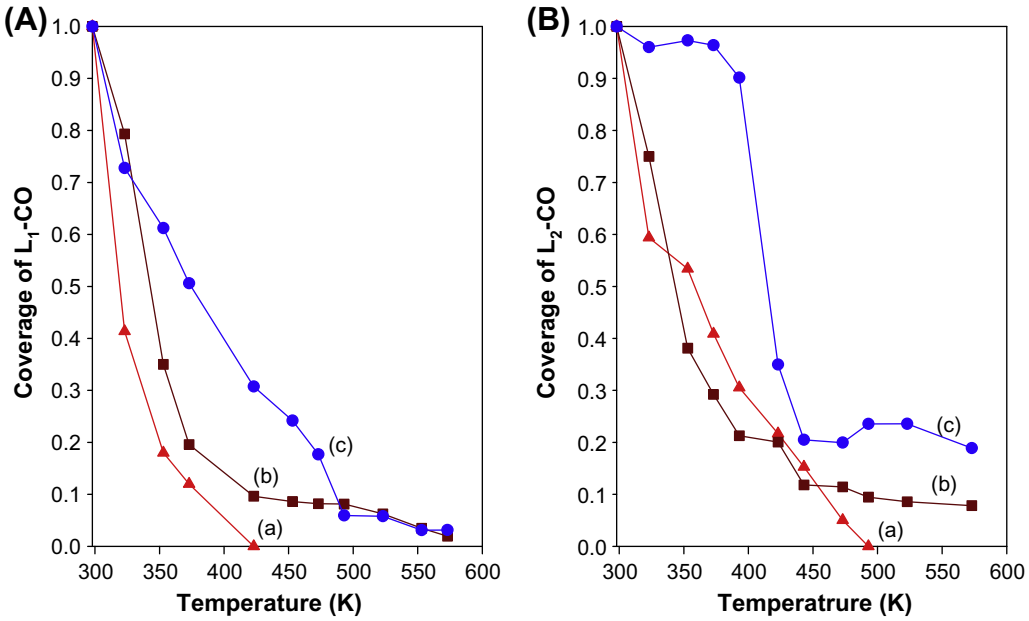

Fig. 6. Changes in the coverage of CO species as a function of temperature on differently pretreated ALE-Cu/SiO_2 catalyst for (A) L_1-CO and (B) L_2-CO: (a) the catalyst after calcination in air at 573 K for 5 h; (b) catalyst reduction at 573 K; (c) catalyst reduction at 773 K. The CO adsorptions were performed by exposure to a 20 ml/min pure CO stream at atmospheric pressure for 30 min, followed by a 20 ml/min helium stream to purge the CO gas for 30 min at 298 K.

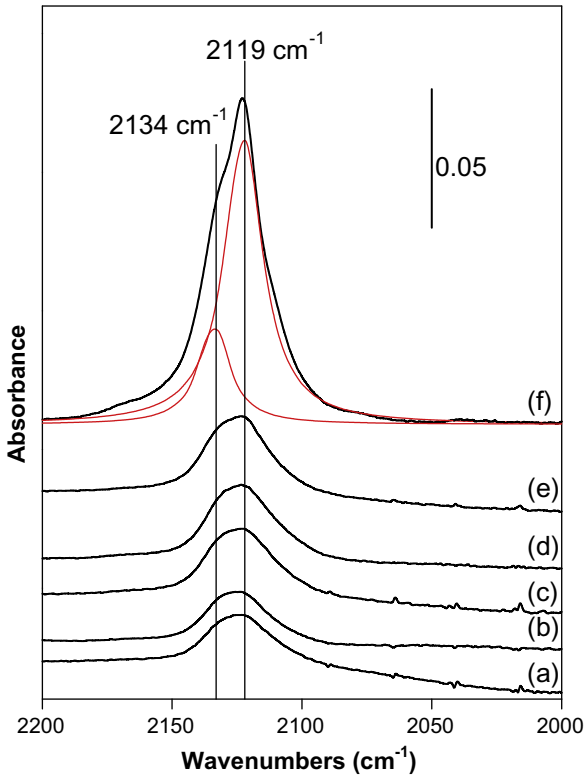

Fig. 7. IR spectra of CO adsorbed onto reduced ALE-Cu/SiO_2 at 298 K with a CO partial pressure of (a) 20.3; (b) 25.3; (c) 50.7; (d) 60.8; (e) 76; (f) 101.3 kPa, respectively.

reduction of Cu^{2+} to Cu^0 [27]. The high-temperature peak in the previous study corresponded to a much higher level of H_2 consumption than the first reduction peak at 512 K. After the reduction of the H_2-TPR process, the ALE-Cu/SiO_2 catalyst was sequentially reduced in H_2 at 773 K for 5 h to achieve a high-temperature reduction. Fig. 4b shows the TPR profile of the high-temperature reduced ALE-Cu/SiO_2 catalyst oxidized by a N_2O stream (20 ml/min) at 353 K for 180 s, revealing two reduction peaks of Cu^+ species at 420 and 673 K in spectrum (b). The TPR profile of the Cu^+ species containing two reduction peaks in Fig. 4b could provide evidence that spectrum (a) involves the one-step reduction of two kinds of Cu oxide. The H_2-TPR profile of SiO_2 support was used as a blank to compare with curves (a) and (b), as shown in Fig. 4c.

The H_2-TPR was further used to study the extent of oxidation of the H_2O preadsorbed ALE-Cu/SiO_2 catalyst. Samples (50 mg) of catalyst were used for H_2O adsorption, which was conducted by feeding a stream of He/H_2O in a 1.1:1 feed molar ratio at 30 ml/min for 1 h at the desired temperature. The catalyst was heated to 573 K under He stream in order to desorb H_2O from the surface after H_2O preadsorption treatment. Fig. 5 reveals the TPR profiles of the effects of H_2O preadsorption and temperature. Curve (a) from the H_2 reduction of the H_2O pretreatment at 298 K shows a broad reduction band at about 413 K. The increasing temperature of H_2O pretreatment apparently promoted oxidation of the ALE-Cu/SiO_2 catalyst, leading to the main reduction temperature shifted to higher temperature and increased H_2 consumption. On the other hand, a weak second reduction peak at about 673 K could be observed in the H_2O preadsorption above 423 K. Compared to the spectrum of reduced ALE-Cu/SiO_2 oxidized by N_2O (Fig. 4b), the TPR peaks in Fig. 5 could be attributed to the reduction of the Cu^+ species, implying that H_2O adsorption might cause partial oxidation of the ALE-Cu/SiO_2 catalyst, even at 298 K.

3.4. FT-IR of CO adsorbed onto ALE-Cu/SiO_2

The IR spectra of CO adsorbed onto the reduced and oxidized ALE-Cu/SiO_2 catalyst obtained with increasing temperature were used to further discuss the assignment of the H_2-TPR peaks in Fig. 4. All experiments were performed by passing a pure CO stream (20 ml/min) over the catalysts for 20 min at 298 K, and then purging the CO with a He stream (20 ml/min) for 50 min. IR spectra of CO adsorption were recorded under the He stream at elevated

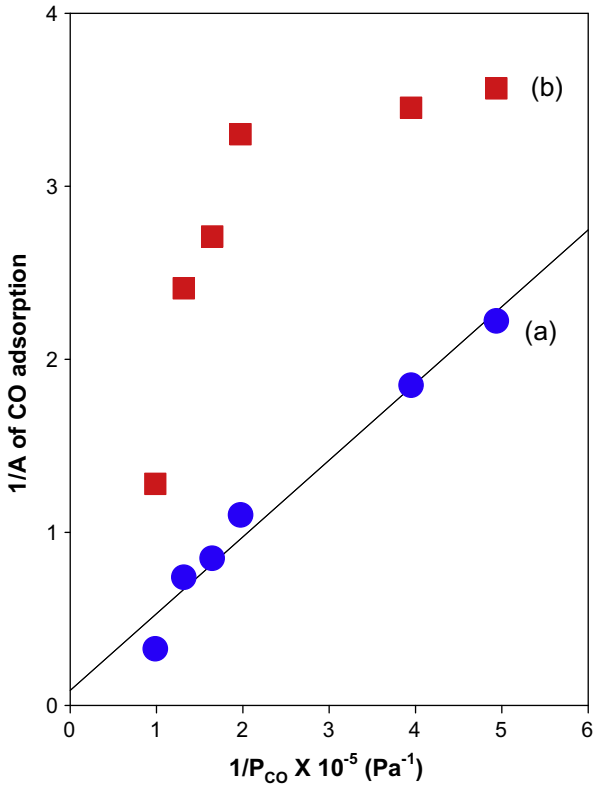

Fig. 8. Dependence of absorbance of the CO species and partial pressure of CO adsorption in Fig. 7: (a) L_1-CO; (b) L_2-CO.

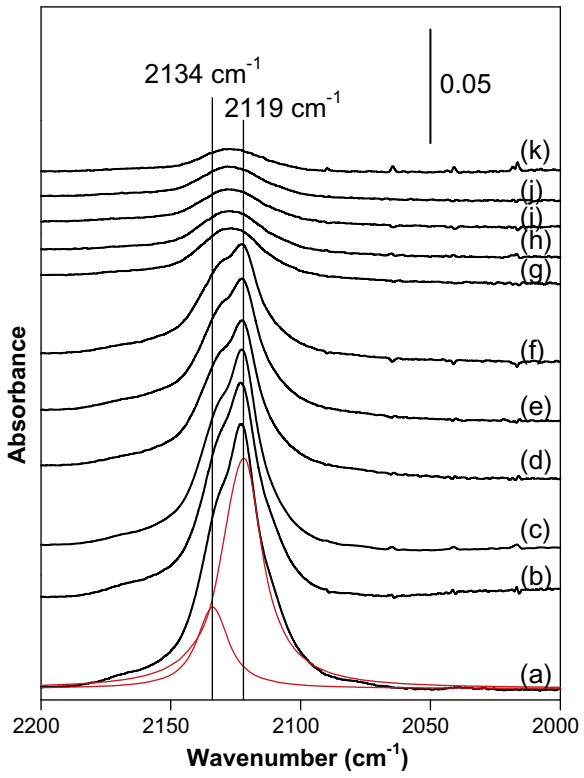

Fig. 9. IR spectra of equilibrium adsorption of CO adsorbed onto reduced ALE-Cu/SiO_2 with varying adsorption temperatures: (a) 298 K; (b) 323 K; (c) 363 K; (d) 373 K; (e) 393 K; (f) 413 K; (g) 433 K; (h) 453 K; (i) 473 K; (j) 493 K; (k) 513 K. The CO adsorptions were performed via exposure to a 20 ml/min pure CO stream at a constant pressure P_{CO} = 101.3 kPa for 30 min, followed by a 20 ml/min helium stream to purge the CO gas for 50 min at the desired temperature.

temperatures. Fig. 6 displays the intensity of the L_1- and L_2-CO species obtained in temperature-dependence studies of the CO adsorbed onto the L_1 and L_2 sites on ALE-Cu/SiO_2 surfaces. The coverage was defined as the ratio A/A_0, where A was the IR band area during temperature increases and A_0 was the initial IR band area of saturated adsorption at 298 K. The change of CO adsorption closely depended on the pretreatments for the ALE-Cu/SiO_2 catalyst. The adsorption of L_1-CO decreased simultaneously with increasing temperature for all ALE-Cu/SiO_2 catalysts (Fig. 6A), showing that oxidized ALE-Cu/SiO_2 without reduction gave poor L_1-CO adsorption. Reduction treatment at 773 K resulted in stronger binding of L_1-CO carbonyl species to the ALE-Cu/SiO_2 catalyst than low-temperature reduction at 573 K. The coverage of the L_2-CO species as a function of temperature is shown in Fig. 6B. The oxidized and low-temperature reduced ALE-Cu/SiO_2 catalyst showed similar declining curves of L_2-CO adsorption with temperature (curves (a) and (b)). The adsorption of L_2-CO was enhanced for the ALE-Cu/SiO_2 catalyst reduced at 773 K (curve (c)), while the peak area of L_2-CO species remained the same over the range 298–383 K. The high-temperature reduction of the ALE-Cu/SiO_2 catalyst at 773 K undoubtedly had a positive effect on L_2-CO adsorption. Considering the H_2-TPR results of the oxidized ALE-Cu/SiO_2 catalyst in Fig. 4a, the peaks of H_2-TPR at 512 and 773 K might be associated with the reduction of Cu^{2+} species at the L_1 and L_2 sites. On the other hand, the reduction of Cu^+ species at 420 and 673 K (Fig. 4b) could also be associated with the reduction of Cu^+ species at the L_1 and L_2 sites.Fig. 7 shows the FT-IR spectra of CO adsorbed onto the reduced ALE-Cu/SiO_2 catalyst with CO partial pressure, indicating evolution of the IR bands of L_1 and L_2-CO species with increased CO partial pressure. The spectra in Fig. 7 were used to further analyze the dependence between intensities of L_1- and L_2-CO adsorption and CO partial pressure. The Langmuir adsorption model gives $\theta_{CO} = \frac{A}{A_0} = \frac{K_{CO}P_{CO}}{1+K_{CO}P_{CO}}$, where K_{CO} is the adsorption coefficient of adsorbed CO species, demonstrating that the dependence between $1/A$ and $1/P_{CO}$ at a constant temperature must appear as a straight line. The CO coverage was determined using the ratio A/A_0, where A was the IR band area at different temperatures and A_0 was the initial IR band area of saturated adsorption at 298 K. The $1/A$ of the L_1- and L_2-CO peaks versus $1/P_{CO}$ are plotted in Fig. 8, showing that the L_1-CO species had a linear relationship, but the L_2-CO species did not. This implied that the adsorption of L_1-CO at 298 K might correspond to the Langmuir adsorption model.

The AEIR method was used to determine the heats of adsorption of the L_1- and L_2-CO species on the ALE-Cu/SiO_2 catalyst [30–40]. Fig. 9 reveals the IR spectra of equilibrium CO adsorbed onto the reduced ALE-Cu/SiO_2 catalyst with different adsorption temperatures. The intensity of IR bands progressively decreased with increasing adsorption temperature. Fig. 10 displays the coverage of the L_1- and L_2-CO species obtained in temperature-dependence studies of the equilibrium CO adsorbed onto the ALE-Cu/SiO_2 surface. The equilibrium adsorption of L_1-CO decreased simultaneously with increasing temperature (Fig. 10A). It was noteworthy that the coverage of the L_2-CO species remained almost constant over the range 298–383 K and then gradually decreased beyond 433 K, as shown in Fig. 10B. The experimental curves in Fig. 10 could be suggested to correspond to the Temkin model, where the values of adsorption heat (E_θ) decrease linearly with the coverage θ ($E_\theta = E_0 - \alpha\theta$) [30–40]. This leads to the generalized expression for the coverage as a function of the adsorption parameter

$$\theta = \frac{RT_a}{\Delta E}\ln\left(\frac{1+K_0P_a}{1+K_1P_a}\right), \quad (1)$$

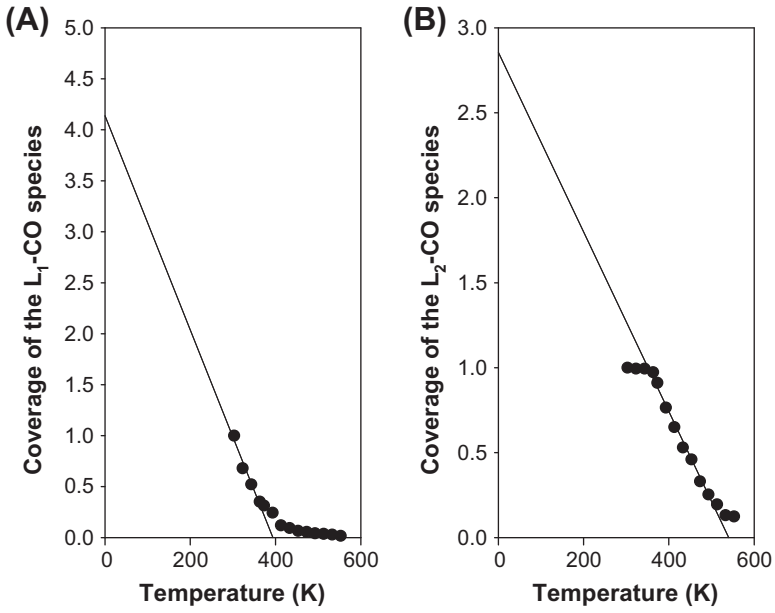

Fig. 10. Change in the coverage of CO species in equilibrium adsorption as a function of the adsorption temperature in Fig. 9: (A) L_1-CO; (B) L_2-CO.

where $\Delta E = E_0 - E_1$ is the difference in the adsorption heat between very small coverage (E_0) and saturation coverage (E_1). K_0 and K_1 are the adsorption coefficients at $\theta = 0$ and $\theta = 1$. Based on the Temkin model, we can assume that $K_0 P_a \gg 1$ and $K_1 P_a \ll 1$, while the adsorption coefficients at $\theta = 0$ can be expressed by $K_0 = A \exp(E_0/RT)$. Thus, Eq. (1) becomes

$$\theta = \left[\frac{R}{E_0 - E_1} \ln(AP_a)\right] T_a + \frac{E_0}{E_0 - E_1}. \quad (2)$$

Eq. (2) corresponds to the linear fraction of the curves in Fig. 10, and the extension of the linear section leads to the θ-axis intercept, with a value of $\frac{E_0}{E_0 - E_1}$. The adsorption coefficients can be derived using statistical thermodynamics, assuming nonactivated and localized CO adsorption [30–40],

$$K_0 = \frac{h^3}{k(2\pi mk)^{3/2}} \frac{1}{T_a^{5/2}} e^{\frac{E_0}{RT_a}} = Ae^{\frac{E_0}{RT_a}}, \quad (3)$$

where h is Plank's constant, k is Boltzmann's constant, and E represents the CO adsorption energy. Eq. (3) determined a pre-exponential factor, A, of 1.7×10^{-12} Pa^{-1} at 300 K. The slopes of the straight lines in Fig. 10 give values of $\Delta E = 12$ kJ/mol for L_1-CO and $\Delta E = 25$ kJ/mol for L_2-CO, assuming that $A = 1.7 \times 10^{-12}$ Pa^{-1}. The interception points of straight lines in Fig. 10A and B represents the values of $E_0/\Delta E$ for L_1- and L_2-CO, leading to $E_0 = 51$ and $E_1 = 39$ kJ/mol for L_1-CO adsorption and $E_0 = 71$ and $E_1 = 46$ kJ/mol for L_2-CO adsorption. The adsorption heat of L_2-CO was obviously higher than that of L_1-CO. This could explain why the L_2 sites have a stronger binding ability for CO than the L_1 sites in our previous study [27].

3.5. Effect of H_2O preadsorption on the WGS reaction

IR spectra in Figs. 1 and 2 show that no detectable intermediates were found in the WGS reaction and that the oxygen atoms formed from H_2O dissociation could rapidly react with CO to generate CO_2. The role of H_2O preadsorption was thus further investigated in the course of the WGS reaction. Fig. 11A compares the WGS reactions on the reduced ALE-Cu/SiO_2 catalysts with and without H_2O preadsorption, giving the interesting results that the activity of the ALE-Cu/SiO_2 catalyst could be significantly enhanced by H_2O preadsorption at 373 K. Fig. 11B also gives the rate of the WGS reaction as a function of the time of H_2O preadsorption, showing a volcano-type dependence of H_2O coverage on activity. One can see that the activity of the ALE-Cu/SiO_2 catalyst generated maximum reaction rates with an increase in the passing time of steam. The TPR profiles in Fig. 5 suggest that the reduced ALE-Cu/SiO_2 catalyst could be partially oxidized by H_2O adsorption at 298–473 K. Therefore, the enhancement of activity by H_2O preadsorption in Fig. 11 was attributed to the partial oxidation on the ALE-Cu/SiO_2 surface.

3.6. Effect of H_2O and CO concentrations on the WGS reaction

Fig. 12 depicts the variation in CO_2 formation rate on the ALE-Cu/SiO_2 catalyst with changes in the concentrations of CO and H_2O at 473 K. The red[1] and blue symbols are the results for constant partial pressures of H_2O and CO, respectively. It is clear that the ALE-Cu/SiO_2 catalyst gave the highest CO_2 formation activity at 3.4 kPa of CO pressure under constant partial pressures of H_2O. Nevertheless, the WGS rate was still slightly enhanced by H_2O concentration under constant partial pressures of CO.

4. Discussion

4.1. Mechanism of the WGS reaction on ALE-Cu/SiO_2

The mechanism of the WGS reaction over Cu-based catalysts has been extensively discussed but remains controversial. Two models, redox and associative mechanisms, have been proposed to explain the mechanism of the WGS reaction on a copper surface. In the associative mechanism, it is suggested that the surface hydroxyls (OH groups) formed from H_2O on a copper surface combine with adsorbed CO to produce reaction intermediates such as formate, carbonate, or carboxyl, which then decompose to H_2 and CO_2 [6,42,43]. The redox mechanism for the WGS reaction involves the oxidation of CO on the surface by atomic oxygen derived from H_2O dissociation [5,44,45]. Studies using density functional

[1] For interpretation of color in Fig. 12, the reader is referred to the web version of this article.

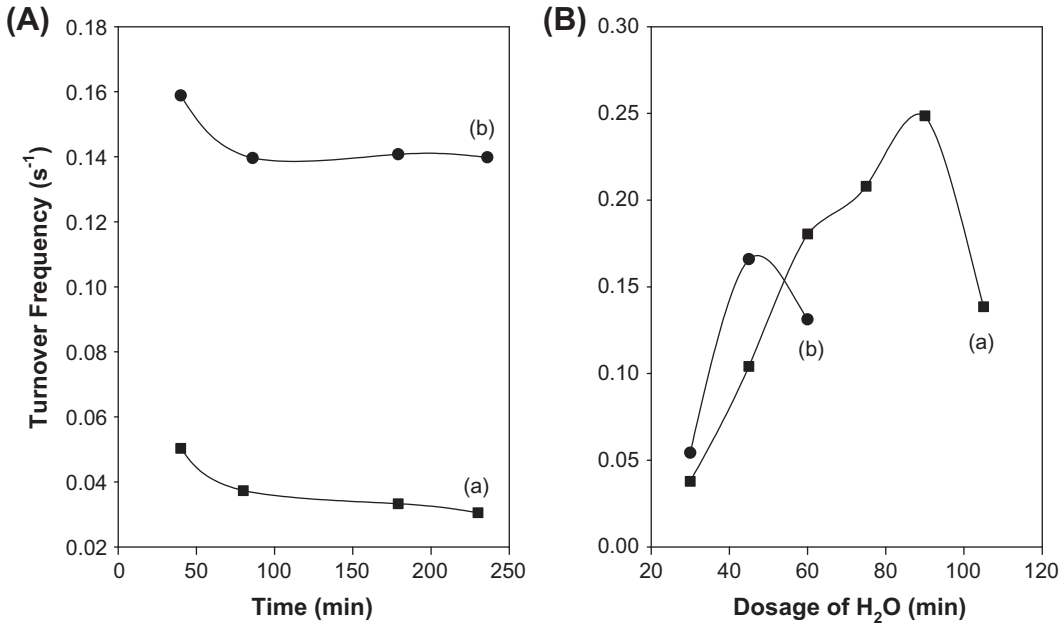

Fig. 11. (A) Comparison of the catalytic activity for the WGS reaction at 373 K on (a) reduced ALE-Cu/SiO_2; (b) H_2O precovered on reduced ALE-Cu/SiO_2. (B) H_2O dosage-dependent WGS reaction on ALE-Cu/SiO_2 at (a) 373 K; (b) 473 K. Precovering of H_2O on reduced ALE-Cu/SiO_2 was performed using a syringe pump that controlled the feeding rate of water at 3 ml/h at the desired temperatures and times. The dosing time of H_2O for the curve (b) in part (A) was 40 min.

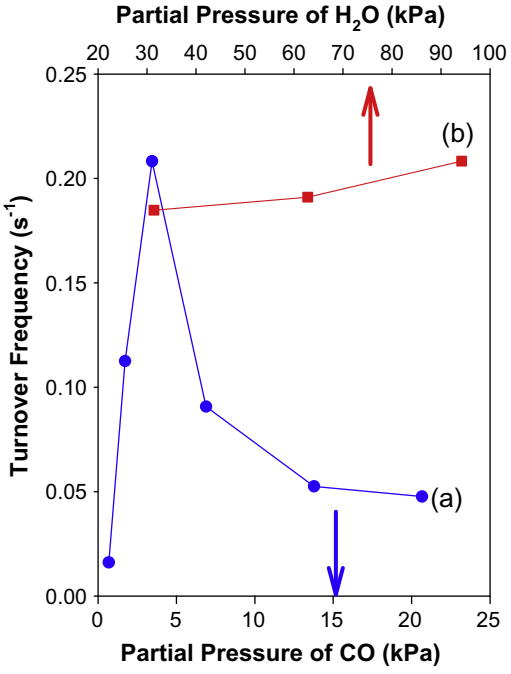

Fig. 12. Dependence of TOF of the WGS reaction on the partial pressure of CO and H_2O on reduced ALE-Cu/SiO_2 at 473 K: (a) various CO partial pressures at a constant pressure of H_2O of 94.2 kPa; (b) various H_2O partial pressures at a constant pressure of CO of 3.4 kPa.

calculations have indicated that the WGS reaction on the Cu surface should proceed following the associative mechanism through a carboxyl intermediate (–COOH) and that the redox mechanism plays no significant role [2,46]. Recently, a new class of Cu catalysts, the so-called low-temperature WGS catalysts based on ceria, have been extensively investigated [4,47]. The formation of oxygen vacancies in the CeO_2 and Cu–$O_{vacancy}$ interface was involved in the generation of active sites to dissociate H_2O [4]. A redox-type mechanism was suggested to dominate the WGS reaction on Cu/CeO_2 in which CO bonded to Cu sites and then reacted with CeO_2 to form CO_2 and oxygen vacancies in CeO_2.

To date, the effect of Cu nanoparticle size on the WGS reaction mechanism has attracted little attention, and few researchers have discussed the catalytic activity and characterization of nanoscale copper particles less than 4 nm in diameter. The above results depicted in Fig. 1 could be interpreted to represent a low likelihood of the WGS reaction proceeding through the intermediate pathway, because no observable reaction intermediates such as formate, carbonate, or carboxyl species were found during the coadsorption of CO and H_2O for the WGS reaction on the ALE-Cu/SiO_2 surface. The IR spectra in Fig. 2 have clearly shown that adsorbed H_2O was readily available to dissociate to atomic oxygen at low temperature. The formation of CO_2 could be ascribed to adsorbed CO species combined with the atomic oxygen. These data provide evidence of a redox-type reaction mechanism on the ALE-Cu/SiO_2 surface. However, water dissociation will always be the essential part of the WGS reaction. In general, copper nanoparticles contain far more low-coordinated corner and edge sites than a flat copper surface and can have better CO binding and water dissociation [43]. The ALE-Cu/SiO_2 catalyst contained two major active sites on the copper surface, sites for L_1-CO and sites for L_2-CO, which could lead water to deeply dissociate to atomic oxygen, as shown in Fig. 5. The transient peak at 1950 cm^{-1} formed from CO and H_2O coadsorption might be ascribed to adsorption of a new carbonyl species (Fig. 1). This peak can be readily vanished through He stream purged (Fig. 1g), implying that this CO species could not be stably adsorbed onto the Cu surface. In general, CO adsorbed onto reduced or oxidized Cu surfaces prefers stable linear adsorption on top sites, giving IR stretching of CO above 2000 cm^{-1} [48]. The bridge type of CO adsorption (IR spectrum below 2000 cm^{-1}) was usually difficult to observe on the Cu surface due to low adsorption energy. Based on the present data, we assume that the formation of a CO peak at 1950 cm^{-1} may be derived from some originally adsorbed CO on L_1 or L_2 sites, strongly affected by coadsorbed oxygen-containing species and/or atomic oxygen from H_2O dissociation. The weak adsorption and red-shifted ν(CO) can be as-

cribed to a σ-component change of the Cu–CO bond [49]. The influence of electron donation by the oxygen-containing species or atomic oxygen acting as a Lewis base at Cu surface sites would decrease σ-bonding between CO and Cu. Thus, these may weaken the CO band and red-shift ν(CO), as the 5σ orbitals of CO are slightly antibonding [49].

4.2. Adsorption heat of CO on ALE-Cu/SiO_2

The AEIR procedure has been used to determine the adsorption heat of CO, which provides useful information for characterizing surface sites on the ALE-Cu/SiO_2 catalyst. The curve in Fig. 10B is obtained with E_0 = 51 and E_1 = 39 kJ/mol for L_1-CO adsorption. By using the slope of curve (a) in Fig. 8 and Eq. (3), we determined the constant heat of adsorption of L_1-CO with E = 41 kJ/mol. The small difference between E_0 and E_1 indicated that the Temkin model for L_1-CO adsorption could correspond to the Langmuir model. E_0 and E_1 for L_2-CO adsorption were found to be 70 and 46 kJ/mol using the Temkin model. Previous research has extensively studied the adsorption heat of CO on Cu^0- and Cu^+-containing solids. Significant energy differences for CO adsorbed onto different Cu^0 surfaces were observed from 18 to 87 kJ/mol [30–33,50]. At low coverage, the adsorption heat of CO on single crystals was ca. 52–65 kJ/mol for Cu(1 0 0), Cu(1 1 0), Cu(2 1 1), Cu(3 1 1), and Cu(1 1 1) [51–57]. Bianchi and coworkers reported E_0 = 82 and E_1 = 57 kJ/mol for a Cu/Al_2O_3 catalyst obtained using the AEIR method [30].

Assignments of the IR bands of CO adsorbed onto a reduced Cu surface have been proposed in the literature [58–60]. In general, IR bands below 2100 cm^{-1} were assigned to CO adsorbed onto low index planes such as the (1 1 1) and (1 0 0) faces [58–60], while the band at 2102–2118 cm^{-1} was assigned to CO adsorbed at imperfect sites, such as step and edge sites. Bands above 2120 cm^{-1} might be from CO adsorbed onto highly dispersed supported copper particles [60–62]. On the other hand, stretching frequencies of CO adsorbed onto copper have also been determined in different regions for each oxidation state. The band of CO adsorbed onto Cu^+ sites has been reported to appear at 2110–2135 cm^{-1} [63]. In this study, the IR spectra of CO adsorbed onto the ALE-Cu/SiO_2 catalyst tended toward higher stretching frequencies of 2122 cm^{-1} (L_1-CO) and 2134 cm^{-1} (L_2-CO), but clear differences were not detected between the L_1- and L_2-CO in terms of the electronic and structural effects of copper. We repeatedly performed TPR experiments on ALE-Cu/SiO_2 samples following high-temperature reduction pretreatment (773 K). No reduction peak was observed in the H_2-TPR experiments for any of the reduced ALE-Cu/SiO_2 catalysts, implying that the sample was likely to have been completely reduced. On the other hand, the adsorption heat of CO can be used to discriminate the CO adsorbed onto different chemical states of the Cu surface. The literature generally indicates that the heat of CO adsorption at Cu^+ sites is higher than that at Cu^0 sites. Cu^+-containing catalysts can increase the heat of CO adsorption to 93–115 kJ/mol [30]. However, the adsorption heats of 39–51 kJ/mol for L_1-CO and 46–70 kJ/mol for L_2-CO might indicate that the CO is bonded to Cu^0 sites on the ALE-Cu/SiO_2 catalyst, according to the adsorption energy of CO–Cu^0 given in the literature [30–33,50–57]. Assignments of IR spectra in the literatures thus suggest that the L_1- and L_2-CO depended on CO adsorbed onto defect sites and onto highly dispersed supported copper particles, respectively.

4.3. Site effect on ALE-Cu/SiO_2 for the WGS reaction

Our previous study has shown that L_1-CO at defect sites (sites giving rise to CO stretching at 2119 cm^{-1}) was highly active in the WGS reaction. The CO adsorbed at L_2 sites, i.e., the small particle and/or isolated copper atom sites, was still available for the WGS reaction, but obviously proved to be less efficient [27]. The results in Fig. 6 show that ALE-Cu/SiO_2 catalysts oxidized and partially reduced at 573 K appeared to show weak adsorption of L_2-CO, but the high-temperature reduction at 773 K evidently induced strong L_2-CO adsorption. Fig. 3B appeared to show that the low-temperature (at 573 K) and high-temperature (at 773 K) reduction treatments were independent of the reaction rate of CO on L_1 sites. However, the sample obtained with low-temperature reduction apparently caused poor activity for L_2-CO (Fig. 3C), because the second peak at 773 K could not be reduced.

Based on these results, reduction of Cu^{2+} species at 512 and 773 K could lead to the generation of reduced L_1 and L_2 sites for CO adsorption. The low-temperature peak at 512 K may correspond to the reduction of Cu^{2+} species on small CuO particles containing defect sites. The second peak at the higher temperature might be attributed to the reduction of Cu^{2+} species that provided strong interaction with the SiO_2 support, while forming sites with highly dispersed Cu particles and/or isolated Cu atoms. Therefore, the TPR peaks at 420 and 673 K in Fig. 4b suggest the reduction of Cu^+ species depending on the L_1 and L_2 sites. Based on the findings described earlier, we concluded that H_2O preadsorption leading to TPR peaks at 373–473 K (Fig. 5) correspond to the reduction of the Cu^+ species on the L_1 sites (413 K), while the weak reduction peak in Fig. 5 was due to the Cu^+ species on the L_2 sites (673 K). The adsorbed H_2O could strongly dissociate to atomic oxygen on the L_1 sites prior to the L_2 sites, even at 298 K, suggesting that adsorbed CO combines with atomic oxygen on the L_1 sites to rapidly form CO_2, as shown by the IR spectra in Fig. 2. This can further explain our previous conclusion that H_2O adsorbed onto defect sites enhances the WGS reaction [27]. Fig. 11 shows that preadsorbed H_2O on the ALE-Cu/SiO_2 catalyst significantly induced a high WGS reaction rate. The enhancement of activity was thus ascribed to the atomic oxygen remaining on the L_1 sites after H_2O dissociation. Fig. 12 reveals the dependence between the CO concentration and the activity of the ALE-Cu/SiO_2 catalyst, indicating that a high CO concentration could cause a low WGS reaction rate. Fig. 3B also shows the consistent phenomenon that the Cu surface through a CO-treatment process with high L_1-CO coverage resulted in a low reaction rate; however, the WGS rate for L_2-CO was independent of its coverage (Fig. 3C). It can be deduced that CO and H_2O should be competitively adsorbed onto the L_1 sites (the defect sites). Although the defect sites were mainly dominated by adsorbed H_2O that deeply dissociated to atomic oxygen in the redox mechanism, preadsorption of CO causing high CO coverage on the defect sites could retard H_2O adsorption.

Dipole–dipole interactions are expected to shift band frequencies toward higher values with increasing CO coverage. The IR spectra of CO adsorption showed the absence of a significant shift of the IR peaks of the L_1- and L_2-CO species with the increase in CO coverage (Fig. 7), indicating that no dipole–dipole coupling of CO occurred on the surface. The defect sites (L_1 sites) are undoubtedly the main active centers for H_2O dissociation over the course of the WGS reaction. Studies using density functional calculations have discussed the mechanism of the WGS reaction on Cu(3 2 1) and Cu(1 1 1) surfaces and obtained some conclusions [2]:

(1) CO reacted with OH^* obtained from H_2O dissociation for an associative mechanism gave a lower activation energy than OH^* further dissociated to provide $O^* + H^*$.
(2) Step sites on the Cu(3 2 1) surface can decrease the activation energy barriers for H_2O dissociation to H and OH, the rate-determining step in the WGS reaction.
(3) The OH radical from water dissociation is more stabilized on the Cu(3 2 1) surface than on the Cu(1 1 1) surface.

Fajín et al. compare the defect site effects of WGS reaction on Cu(3 2 1) and Cu(1 1 1) surfaces, showing that the rough Cu surface can cause more imperfect sites to enhance H_2O dissociation [2]. However, our results for Cu nanoparticles and the ALE-Cu/SiO_2 catalyst indicated very different reaction behavior for WGS from the studies described above. The Cu nanoparticles in this paper mainly contained defect sites, and isolated sites on surface dramatically enhanced strong H_2O dissociation, resulting in the formation of adsorbed O^* on the defect sites and leading to the redox pathway (see Fig. 2). The step of H_2O dissociation to generate O^* on the L_1 sites was suggested to be the rate-determining step during the WGS reaction. The O^* on the L_1 sites provided high chemical activity to convert the L_1- and L_2-CO species for CO_2 generation.

In general, CO is generally desorbed from Cu surfaces below room temperature because CO weakly bonds with the Cu surface [50]. Nevertheless, the ALE-Cu/SiO_2 catalyst showed a strong ability for CO adsorption, with two desorption peaks at approximately 343–353 and 443–463 K during the CO-TPD process [8]. Some authors have indicated that defect sites can provide larger binding energy for CO adsorption than the sites on a flat surface [2,64,65]. A comparison of the IR spectra of CO adsorbed onto ALE-Cu/SiO_2 with respect to temperature suggests that the low-temperature (343–353 K) and high-temperature (443–463 K) peaks for CO desorption should reflect the CO adsorbed onto L_1 and L_2 sites, respectively. The IR spectra of CO adsorbed onto ALE-Cu/SiO_2 also tend to show higher CO stretching energy, implying that the Cu nanoparticles provide many more L_1 and L_2 sites to bind CO. The dispersal of the Cu particles might reduce the possibility of obtaining a large flat structure, as evidenced by the absence of low vibrational energy below 2100 cm^{-1}.

We could observe that E_0 slightly varied with the coverage of the L_1-CO. To our knowledge, there have been no reports in the literature that transition metal surfaces such as those of Cu, Au, Pt, Ir, Pd, and Pt–Rh could show such a small difference between E_0 and E_1 for CO adsorption using a Langmuir adsorption model [30–40]. The adsorption heat for very low CO coverage (E_0) is usually high enough to allow the population of this state under equilibrium conditions, whereas CO population becomes more difficult with increasing CO coverage. In the present study, the CO coverage did not seem to affect the CO population at L_1 sites significantly, while the L_2 sites might give high activation energy for CO desorption, leading to very small differences in CO coverage at 298–383 K.

5. Conclusions

In this paper, we discussed the reaction mechanism, the role of active sites and the site properties for the WGS reaction on the ALE-Cu/SiO_2 catalyst. The ALE-Cu/SiO_2 catalyst contained two major active sites on the copper surface: sites for L_1-CO and sites with highly dispersed Cu particles and/or isolated Cu atoms (sites for L_2-CO). The reduction peaks of the Cu^{2+} species at 512 and 773 K in the TPR profiles are proposed to depend on the generation of reduced L_1 and L_2 sites for CO adsorption.

It has been shown that the defect sites play an important role over the course of the WGS reaction, as they mainly dominate the adsorbed H_2O that is deeply dissociated to atomic oxygen in the redox mechanism. CO and H_2O are proposed to competitively adsorb onto the defect sites. The ALE-Cu/SiO_2 catalyst can dramatically enhance strong H_2O dissociation and form adsorbed atomic oxygen (O^*) derived from H_2O on the defect sites, leading to high reactivity of the O^* on defect sites toward L_1- and L_2-CO species to form CO_2. The step of H_2O dissociation to generate O^* on defect sites is suggested to be the rate-determining step during the WGS reaction.

The adsorption heats of CO adsorbed onto L_1 and L_2 sites are obtained by the AEIR method. The heats of L_2-CO vary linearly with coverage from 46 to 70 kJ/mol at $\theta = 1$ and $\theta = 0$, respectively. The adsorption heats of L_1-CO are obtained with $E_0 = 51$ and $E_1 = 39$ kJ/mol. The small difference between E_0 and E_1 suggests that the Temkin model for L_1-CO adsorption is in accordance with the Langmuir model.

Acknowledgments

Financial support from the National Science Council of the Republic of China (NSC 98-2113-M-182-001-MY2) is gratefully acknowledged. Dr. Pin C. Yao is acknowledged for operating the F-120C ALE equipment in the material and chemical research laboratories at the Industrial Technology Research Institute.

References

[1] N. Ínoğlu, R. Kitchin, J. Catal. 261 (2009) 188.
[2] J.L.C. Fajín, M.N.D.S. Cordeiro, F. Illas, J.R.B. Gomes, J. Catal. 268 (2009) 131.
[3] M. Rønning, F. Huber, H. Meland, H. Venvik, D. Chen, A. Holmen, Catal. Today 100 (2005) 249.
[4] X. Wang, J.A. Rodriguez, J.C. Hanson, D. Gamarra, A. Martínez-Arias, M. Fernández-García, J. Phys. Chem. B 110 (2006) 428.
[5] N.A. Koryabkina, A.A. Phatak, W.F. Ruettinger, R.J. Farrauto, F.H. Ribeiro, J. Catal. 217 (2003) 233.
[6] C.V. Ovesen, B.S. Clausen, B.S. Hammershøi, G. Steffensen, T. Askgaard, I. Chorkendorff, J.K. Nørskov, P.B. Rasmussen, P. Stoltze, P. Taylor, J. Catal. 158 (1996) 170.
[7] C. Ratnasamy, J.P. Wagner, Catal. Rev. Sci. Eng. 51 (2009) 325.
[8] C.S. Chen, J.H. Lin, J.H. You, C.R. Chen, J. Am. Chem. Soc. 128 (2006) 15950.
[9] C.S. Chen, W.H. Cheng, S.S. Lin, Appl. Catal. A 257 (2004) 97.
[10] C.S. Chen, W.H. Cheng, S.S. Lin, Appl. Catal. A 238 (2003) 55.
[11] C.S. Chen, W.H. Cheng, Catal. Lett. 83 (2002) 121.
[12] C.S. Chen, W.H. Cheng, S.S. Lin, Chem. Commun. (2001) 1770.
[13] C.S. Chen, W.H. Cheng, S.S. Lin, Catal. Lett. 68 (2000) 45.
[14] R. Burch, Phys. Chem. Chem. Phys. 8 (2006) 5483.
[15] H. Yahiro, K. Murawaki, K. Saiki, T. Yamamoto, H. Yamaura, Catal. Today 126 (2007) 436.
[16] J.A. Rodriguez, P. Liua, J. Hrbek, M. Perez, J. Evans, J. Mol. Catal. A 281 (2008) 59.
[17] P. Kumar, R. Idem, Energy Fuels 21 (2007) 522.
[18] J.A. Rodriguez, P. Liu, X. Wang, W. Wen, J. Hanson, J. Hrbek, M. Perez, J. Evans, Catal. Today 143 (2009) 45.
[19] J.A. Rodriguez, P. Liu, J. Hrbek, J. Evans, M. Pérez, Angew. Chem. Int. Ed. 46 (2007) 1329.
[20] J. Knudsen, A.U. Nilekar, R.T. Vang, J. Schnadt, E.L. Kunkes, J.A. Dumesic, M. Mavrikakis, F. Besenbacher, J. Am. Chem. Soc. 129 (2007) 6485.
[21] Y. Chen, J. Cheng, P. Hu, H. Wang, Surf. Sci. 602 (2008) 2828.
[22] B. White, M. Yin, A. Hall, D. Le, S. Stolbov, T. Rahman, N. Turro, S. O'Brien, Nano Lett. 6 (2006) 2095.
[23] J.S. Garitaonandia, M. Insausti, E. Goikolea, M. Suzuki, J.D. Cashion, N. Kawamura, H. Ohsawa, I.G.D. Muro, K. Suzuki, F. Plazaola, T. Rojo, Nano Lett. 8 (2008) 661.
[24] Z. Pászti, G. Petö, Z.E. Horváth, A. Karacs, L. Guczi, J. Phys. Chem. B 101 (1997) 2109.
[25] P. Chen, X. Wu, J. Lin, K.L. Tan, J. Phys. Chem. B 103 (1999) 4559.
[26] L. Porte, M. Phaner-Goutorbe, J.M. Guigner, J.C. Bertolini, Surf. Sci. 424 (1999) 262.
[27] C.S. Chen, J.H. Lin, T.W. Lai, B.H. Li, J. Catal. 263 (2009) 155.
[28] C.S. Chen, J.H. Lin, T.W. Lai, Chem. Commun. (2008) 4983.
[29] B.S. Lim, A. Rahtu, G. Gordon, Nat. Mater. 2 (2003) 749.
[30] O. Dulaurent, X. Courtois, V. Perrichon, D. Bianchi, J. Phys. Chem. B 104 (2000) 6001.
[31] S. Zeradine, A. Bourane, D. Bianchi, J. Phys. Chem. B 105 (2001) 7254.
[32] S. Derrouiche, D. Bianchi, Langmuir 20 (2004) 4489.
[33] S. Derrouiche, V. Perrichon, D. Bianchi, J. Phys. Chem. B 107 (2003) 8588.
[34] S. Derrouiche, P. Gravejat, D. Bianchi, J. Am. Chem. Soc. 126 (2004) 13010.
[35] A. Bourane, O. Dulaurent, D. Bianchi, Langmuir 17 (2001) 5496.
[36] T. Chafik, O. Dulaurent, J.L. Gass, D. Bianchi, J. Catal. 179 (1998) 503.
[37] O. Dulaurent, K. Chandes, C. Bouly, D. Bianchi, J. Catal. 188 (1999) 237.
[38] P. Gravejat, S. Derrouiche, D. Farrussengn, K. Lombaert, C. Mirodatos, D. Bianchi, J. Phys. Chem. C 111 (2007) 9496.
[39] A. Bourane, M. Nawdali, D. Bianchi, J. Phys. Chem. B 106 (2002) 2665.
[40] O. Dulaurent, D. Bianchi, Appl. Catal. A 196 (2000) 271.
[41] J. Nakamura, I. Nakamura, T. Uchijima, Y. Kanai, T. Watanabe, M. Saito, T. Fujitani, J. Catal. 160 (1996) 65.
[42] C.T. Campbell, K.A. Daube, J. Catal. 104 (1987) 109.
[43] P. Liu, J. Rodriquez, J. Chem. Phys. 126 (2007) 164705.
[44] D.S. Newsome, Catal. Rev. Sci. Eng. 21 (1980) 275.
[45] E. Fiolitakis, H. Hofmann, J. Catal. 80 (1983) 328.
[46] A.A. Gokhale, J.A. Dumesic, M. Mavrikakis, J. Am. Chem. Soc. 130 (2008) 1402.

[47] J.A. Rodriguez, J.G. raciani, J. Evans, J.B. Park, F. Yang, D. Stacchiola, S.D. Senanayake, S. Ma, M. Pérez, P. Liu, J.F. Sanz, J. Hrbek, Angew. Chem. Int. Ed. 48 (2009) 8047.
[48] J. Radnik, H.J. Ernst, J. Chem. Phys. 110 (1999) 10522.
[49] F. Coloma, B.B. Baeza, C.H. Rochester, J.A. Anderson, Phys. Chem. Chem. Phys. 3 (2001) 4817.
[50] M.J. Sandoval, A.T. Bell, J. Catal. 144 (1993) 227.
[51] K. Horn, M. Hussain, J. Pritchard, Surf. Sci. 63 (1977) 244.
[52] I.E. Wachs, R.J. Madix, J. Catal. 53 (1978) 208.
[53] M. Christiansen, E.V. Thomsen, J. Onsgaard, Surf. Sci. 261 (1992) 179.
[54] H. Papp, J. Pritchard, Surf. Sci. 53 (1975) 371.
[55] J. Kessler, F. Thieme, Surf. Sci. 67 (1977) 405.
[56] P. Hollins, J. Pritchard, Surf. Sci. 89 (1979) 486.
[57] C.M. Truong, J.A. Rodriguez, D.W. Goodman, Surf. Sci. Lett. 271 (1992) L385.
[58] P. Hollins, Surf. Sci. Rep. 16 (1992) 51.
[59] F. Boccuzzi, A. Chiorino, G. Martra, M. Gargano, N. Ravasio, B. Carrozzini, J. Catal. 165 (1997) 129.
[60] F. Coloma, F. Marquez, C.H. Rochester, J.A. Anderson, Phys. Chem. Chem. Phys. 2 (2000) 5320.
[61] F. Boccuzzi, S. Coluccia, G. Martra, N. Ravasio, J. Catal. 184 (1999) 316.
[62] F. Boccuzzi, G. Martra, C. Partipilo Papalia, N. Ravasio, J. Catal. 184 (1999) 334.
[63] A. Dandekar, M.A. Vannice, J. Catal. 178 (1998) 621.
[64] J. Braun, A.P. Graham, F. Hofmann, W. Silvestri, J.P. Toennies, G. Witte, J. Chem. Phys. 105 (1996) 3258.
[65] S. Vollmer, G. Witte, C. Wöll, Catal. Lett. 77 (2001) 97.